Macromolecular Chemistry and Physics
www.mcp-journal.de

Hydrophilic $(AB)_n$ Segmented Copolymers for Melt Extrusion-Based Additive Manufacturing

Jannik Mechau, Andreas Frank, Ezgi Bakirci, Simon Gumbel, Tomasz Jungst, Reiner Giesa, Jürgen Groll, Paul D. Dalton, and Hans-Werner Schmidt**

Several manufacturing technologies beneficially involve processing from the melt, including extrusion-based printing, electrospinning, and electrohydrodynamic jetting. In this study, $(AB)_n$ segmented copolymers are tailored for melt-processing to form physically crosslinked hydrogels after swelling. The copolymers are composed of hydrophilic poly(ethylene glycol)-based segments and hydrophobic bisurea segments, which form physical crosslinks via hydrogen bonds. The degree of polymerization was adjusted to match the melt viscosity to the different melt-processing techniques. Using extrusion-based printing, a width of approximately 260 µm is printed into 3D constructs, with excellent interlayer bonding at fiber junctions, due to hydrogen bonding between the layers. For melt electrospinning, much thinner fibers in the range of about 1–15 µm are obtained and produced in a typical nonwoven morphology. With melt electrowriting, fibers are deposited in a controlled way to well-defined 3D constructs. In this case, multiple fiber layers fuse together enabling constructs with line width in the range of 70 to 160 µm. If exposed to water the printed constructs swell and form physically crosslinked hydrogels that slowly disintegrate, which is a feature for soluble inks within biofabrication strategies. In this context, cytotoxicity tests confirm the viability of cells and thus demonstrating biocompatibility of this class of copolymers.

1. Introduction

Extrusion-based printing (EBP) of polymer melts (including fused filament fabrication) is the most inexpensive and readily accessed method for additive manufacturing (AM).[1] Other well-known AM technologies such as electron beam melting[2] and selective laser sintering[3] involve melt processing to form their final products; however, they are less accessible due to printer costs. In AM, melt processing is a sustainable approach to avoid the use of solvents for product fabrication in a diverse range of end uses.[4]

Considering the diversity of final applications for EBP, the range of printable materials available for processing remains limited. The vast majority of materials already used for EBP are either poly(lactic acid) (PLA), poly(acrylonitrile-butadiene-styrene),[5] or poly(ethylene terephthalate glycol), while polypropylene (PP),[6,7] poly(ε-caprolactone) (PCL),[8] polycarbonate,[5] poly(ether ether ketone),[9] and nylon[6] have also been developed. This study is aimed at expanding the number of melt-processed materials that can subsequently form hydrogels and then slowly disintegrate, which is of interest for biofabrication strategies. In **Figure 1**, the techniques EBP, melt electrospinning (MES), and melt electrowriting (MEW) are shown schematically. EBP requires the extrusion of a polymer melt through a nozzle directly onto a translating build plate. However, at smaller nozzle diameters of 100 µm and below, a processing phenomenon called "die swell" predominates that limits smaller extruded fiber sizes.[10] Therefore, the EBP of melts has a practical lower limit in printed diameter that is difficult to overcome.

Substantially smaller diameter fibers than EBP can be generated using MES (Figure 1B), although electrical instabilities mean that accurate fiber placement is difficult to control. In this manufacturing process, there is a several centimeter gap between the nozzle and build plate (respectively called translating collector) and high voltages are applied to initiate electrical instabilities (termed whipping), to stretch the molten jet into smaller dimensions. The fibers for MES have been reported from 500 nm up to low-micron diameters, and common polymers and polymer blends[11] such as PCL, PLA, and PP with different additives are used.[12]

J. Mechau, A. Frank, S. Gumbel, Dr. R. Giesa, Prof. H.-W. Schmidt
Macromolecular Chemistry and Bavarian Polymer Institute (BPI)
University of Bayreuth
Universitätsstraße 30, Bayreuth 95440, Germany
E-mail: hans-werner.schmidt@uni-bayreuth.de
E. Bakirci, Dr. T. Jungst, Prof. J. Groll, Prof. P. D. Dalton
Department for Functional Materials in Medicine and Dentistry and Bavarian Polymer Institute (BPI)
University Würzburg
Pleicherwall 2, Würzburg 97070, Germany
E-mail: paul.dalton@fmz.uni-wuerzburg.de
The ORCID identification number(s) for the author(s) of this article can be found under https://doi.org/10.1002/macp.202000265.

DOI: 10.1002/macp.202000265

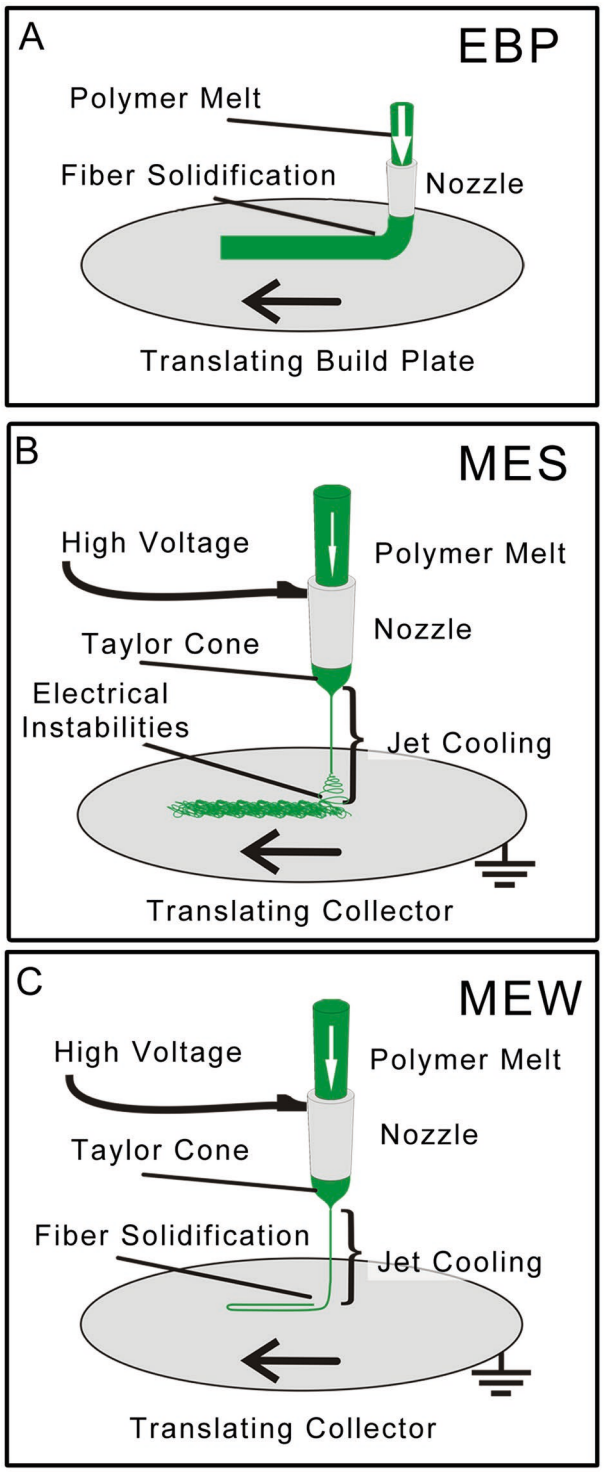

Figure 1. Schematic of the three melt extrusion-based AM technologies used in this study for the $(AB)_n$ segmented copolymers. EBP is the most common AM technology and involves extruding onto a build plate. MES involves a larger diameter nozzle that is charged with an applied voltage and is raised above an earthed collector. MEW does not have electrical instabilities due to lower applied high voltages and a higher flow rate to the nozzle than MES. The approximate magnitude of the flow rate for each processing technology is indicated with the white arrow thicknesses.

Filling this dimensional gap between EBP and MES, it is possible to make intermediate diameter filaments using MEW (Figure 1C).[11] With this technique, a molten fluid column, or jet, at a low flow rate can be electrically stabilized and direct-written onto a translating collector. Depending on the flow rate to the nozzle, MEW can produce defined low-micron and sub-micrometer scale fibers, typically from 100 µm down to 0.8 µm.[13] The MEW process has been primarily developed with the hydrophobic PCL due to its low melting temperature of 60 °C and its long-term thermal stability.[14–16] Previous studies showed that the combination of hydrogels with reinforcing MEW structures of PCL adjusts mechanical properties and dimensional stability.[17,18]

All of the three aforementioned melt processing technologies described above are limited in producing stable hydrogels or hydrogels that disintegrate/dissolve in water with time. Hydrogels and water-soluble polymers are an important class of materials that are the basis for numerous household products and are used widely in biomedical applications, having utility as contact lenses, drug delivery systems, biomaterials, and as research tools.

In this context, the central goal of this work is the synthesis of $(AB)_n$ segmented copolymers with hydrophilic poly(ethylene glycol) (PEG)-based segments and bisurea segments that can form physical crosslinks and melt processed by using EBP, MES, and MEW to prepare 3D constructs. Such fabricated materials can then be swollen or disintegrated with water depending on the chemical structure. This provides utility for different biofabrication paradigms, including fabrication of microchannels,[19] biopaper,[20] or as a temporary barrier for matrix casting.

Therefore, the $(AB)_n$ segmented copolymers require the following property profile: 1) printable from the melt at moderate temperatures; 2) long-term melt stability at the printing temperature; and 3) adjustable swelling and dissolution properties. Additionally, in view of potential biofabrication applications where this material is used in the presence of cells, the polymers should not be cytotoxic. The intention of such polymers is therefore not as conventional cell adhesive scaffolds, but to produce a temporary structure that helps in the hierarchical formation of biological tissues, or biofabrication.[21]

Dankers et al. synthesized $(AB)_n$ and ABA segmented copolymers based on PEG segments and ureido-pyrimidone (UPy) moieties for intrarenal drug delivery systems after subcapsular implantation.[22] These copolymers form supramolecular hydrogels from mixtures of water and organic solvents. Guo et al. expanded this architecture concept with multiblock PEG-based copolymers with UPy in the backbone and realized stimuli-responsive supramolecular hydrogels.[23] Pawar et al. investigated PEG-based $(AB)_n$ segmented copolymers with bisurea segments as biocompatible, injectable hydrogels with shear-thinning behavior.[24] The properties of the hydrogels can be tailored due to the length of the hydrophilic PEG segments and the physical crosslink density of the hydrophobic bisurea hard segments.[24] An improvement in mechanical and stretchable properties was demonstrated by Cui et al. by shortening the length of the PEG segment and using an aliphatic dodecyl spacer.[25] The hydrophobic dodecyl spacers shield the urea groups from water. Due to the relatively large spacer, the hydrogel is insoluble in water, but can be dissolved in organic solvents and processed by solution casting or electrospinning in hydrogel films or nanofibers.[25] All

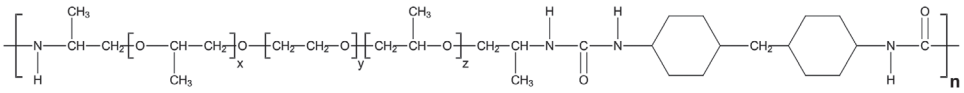

1a - d

Figure 2. $(AB)_n$ segmented copolymers **1a–1d** based on hydrophilic PEG containing segments and bisurea segments investigated in view of melt processing.

the above-described polymers are processed from solution and no information is given on melt processing and in view of AM.

Herein, we report on $(AB)_n$ segmented copolymers tailored for EBP, MES, and MEW. These polymers have hydrophilic poly(propylene glycol)-terminated poly(ethylene glycol) segments (PPG-PEG-PPG) and methylene-bis-cyclohexyl bisurea segments as shown in **Figure 2**. The degree of polymerization n was varied to adjust the melt viscosity, required by the different applied melt processing techniques. With each processing technique, different constructs with different dimensions and resolutions were prepared and exposed to water. In view of biofabrication, cytotoxicity tests were performed.

2. Results and Discussion

2.1. Synthesis and Characterization

For the synthesis of bisurea-based $(AB)_n$ segmented copolymers, diamines and diisocyanates are used as building blocks. A PPG-PEG-PPG diamine with a molecular weight of 900 g mol^{-1} was used as hydrophilic segments and 4,4′-methylene-bis-cyclohexylisocyanate was used as hydrophobic segments. The synthesis and purification of the $(AB)_n$ segmented copolymers **1a–1d** is described in detail in the Supporting Information and Figures S1–S3, Supporting Information. The polymers differ in the degree of polymerization n and thus in the molecular weight. The processing temperature for melt extrusion-based AM technologies depends strongly on the molecular weight (see **Table 1**). To adjust the molecular weight, the amount of n-butylamine was varied from 0 to 20 mol%, resulting in a number average molar mass $\overline{M}_n$ from around 44–31 kg mol^{-1} for **1a–1d**, respectively. The dispersity ranges between 1.6 and 1.7 that is low for step-growth polymerizations. However, the low dispersity was achieved due to the purification via dialysis (see S3, Supporting Information). Such narrow molecular weight distributions were also previously reported for similar $(AB)_n$ segmented copolymers with PEG segments.[24]

Table 1. Size exclusion chromatography (SEC) data of $(AB)_n$ segmented copolymers **1a–1d**.

Polymer	Amount of n-butylamine[mol%]	$\overline{M}_n$[a)][kg mol^{-1}]	$\overline{M}_w$[b)][kg mol^{-1}]	$Đ$[c)]
1a	0	43.8	68.7	1.6
1b	5	39.6	65.2	1.7
1c	10	37.0	59.2	1.6
1d	20	30.8	52.4	1.7

$\overline{M}_n$ and $\overline{M}_w$ were determined by SEC; eluent THF+0.25 wt% TBAB; polystyrene calibration; [a)]$\overline{M}_n$: number average molar mass; [b)]$\overline{M}_w$: weight average molar mass; [c)]$Đ$: dispersity.

In view of melt processing these polymers, the investigation of thermal properties is mandatory. Therefore, thermal analysis was conducted by differential scanning calorimetry (DSC), dynamical mechanical thermal analysis (DMTA), and rheology. DSC reveals a glass transition (T_g) at around –45 °C for all four polymers **1a–1d**. No melting or crystallization peak was observed as shown for **1c** in Figure S4, Supporting Information, confirming that the PPG-PEG-PPG segment is completely amorphous. Several previous studies suggest that

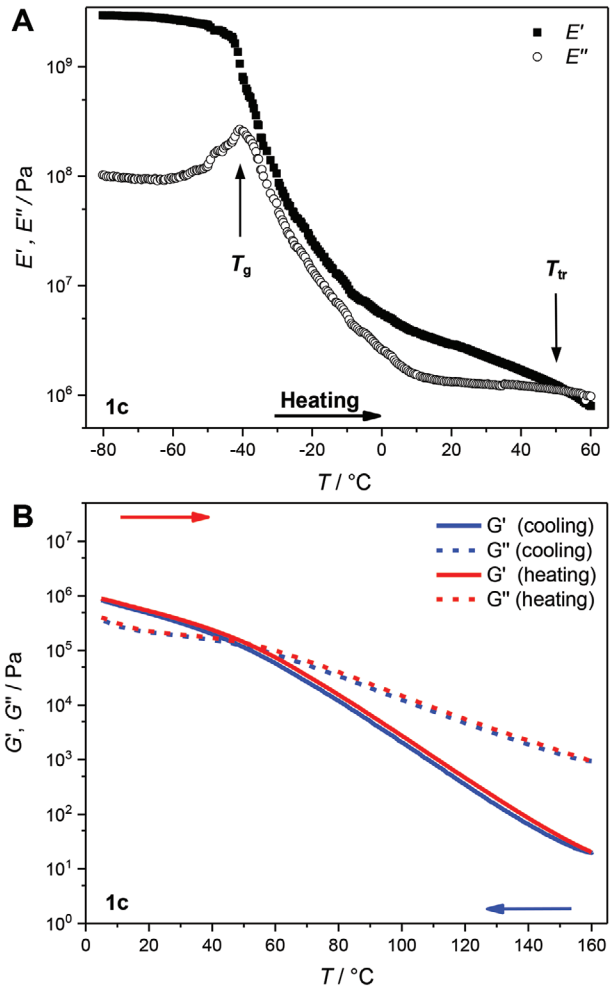

Figure 3. A) Dynamic mechanical thermal analysis of **1c** (tension geometry: heating rate: 2 K min^{-1}, frequency: 1 Hz). Maximum of the loss modulus at –41 °C corresponds to the T_g of the PPG-PEG-PPG segments. The T_{tr} from elastic to viscous behavior occurs at 53 °C. B) Oscillation rheology measurement shows the transition between elastic and viscous behavior at 48 °C upon cooling and 51 °C upon heating (cooling and heating rate: 2 K min^{-1}, frequency: 1 Hz).

PEG segments with higher molecular weight lacking pendent PPG units are semicrystalline and hence show a melting and crystallization transition in $(AB)_n$ segmented copolymers.[23,24] Disassemble and reassembly of urea hydrogen bonds are not detected in the DSC. DMTA of **1c** in a tension geometry indicates a glass transition at –41 °C indicated by the maximum of the loss modulus (E'') (**Figure 3**A), correlating well with the value determined in the DSC. By further heating to 20 °C, the elastic modulus decreases by almost three orders of magnitude compared to the value at the T_g from around 3 GPa to around 3 MPa, revealing a soft material at room temperature. However, the storage modulus (E') is above the loss modulus (E'') and thus the polymer remains in the solid state due to the physical crosslinks. The transition temperature (T_{tr}) from elastic to viscous behavior is indicated by the intersection of storage and loss modulus at around 53 °C that can be explained by the disassembly of the bisurea hydrogen bonds. Temperature-dependent oscillation rheology of **1c** reveals a transition between elastic (G') and viscous (G'') shear modulus at 51 and 48 °C upon heating and cooling, respectively (Figure 3B). Then upon heating, a steady decrease of elastic and viscous modulus between 40 and 160 °C was recorded. This effect is reversible as shown by a close superposition of cooling and heating curve. Therefore, the physical network between the urea moieties is formed again upon cooling to room temperature. Similar behavior is shown for **1b** and **1d** in Figure S5, Supporting Information. With decreasing molecular weight, the transition between G' and G'' from **1b** to **1d** is shifted to lower temperatures from 74 to 34°C upon cooling.

An essential parameter for AM is the polymer melt viscosity at the processing temperature that has to be sufficiently low to extrude the polymer through a fine nozzle.[26] Therefore, the complex melt viscosity (η^*) of the polymers upon cooling from the melt was measured to determine the viscosity as function of molecular weight. As expected,[27] the melt viscosity for each polymer **1b**–**1d** is proportional to its molecular weight (**Figure 4**A). Upon cooling, all viscosity curves show a steady increase by three orders of magnitude between 140 and 50 °C. At ≈40 °C, a change in the slope is observed that is explained by the progression reaggregation of the hydrogen bonds of the urea groups resulting in an elastic material.

In addition to the optimal viscosity, the thermal stability at the melt processing temperature is essential to avoid thermal degradation of the polymer during printing. Previous studies with a related $(AB)_n$ segmented copolymer possessing siloxane-based soft and hexamethylene-bisurea hard segment reveal irreversible thermal degradation of the urea units above 140 °C due to crosslink reactions indicated by an increase in melt viscosity.[28] Isothermal rotational viscosity measurements of **1d** at 100 and 120 °C resulted in constant melt viscosities around 700 and 90 Pa s, respectively, over an extended period of 20 h that exceeds the printing time of 1–2 h (Figure 4B). Consequently, the fiber diameter will not be affected within the printing time by varying polymer melt viscosity.

Increasing amounts of the regulator *n*-butylamine lower the molecular weight of the polymer as expected. Furthermore, with lower molecular weight, a decrease in the transition temperatures determined by oscillation rheology measurements is

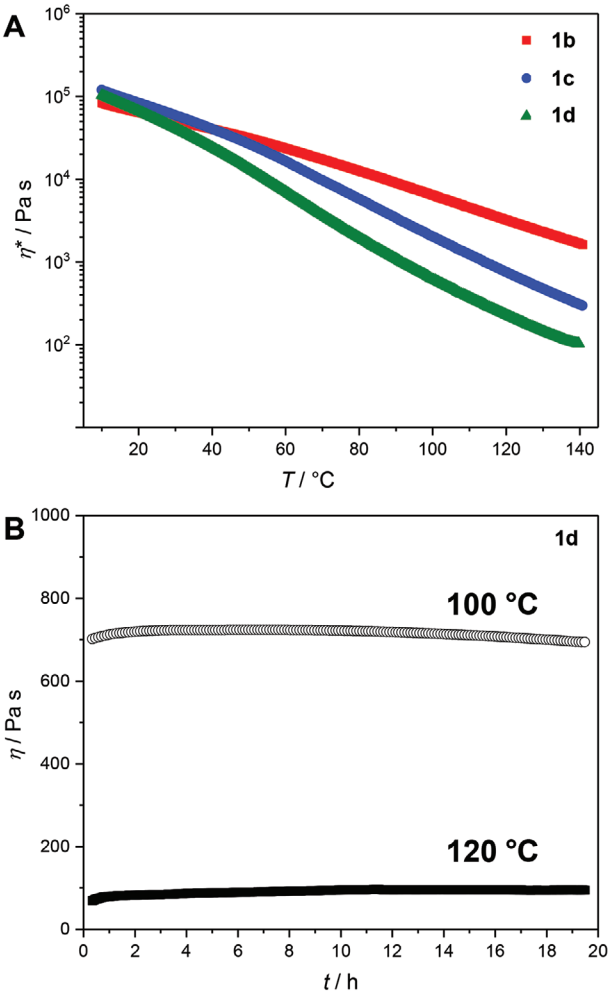

Figure 4. A) Complex melt viscosity of **1b**, **1c**, and **1d** upon cooling (2 K min^{-1}, 1 Hz, 0.05%). B) Time-depending rotational viscosity measurement of **1d** at 100 and 120 °C for 20 h, indicating no significant change in melt viscosity (0.08 rad).

detected. The drop in the transition temperature, upon cooling, from **1b**, **1c** to **1d** is from 74, 48 to 34°C, respectively. Therefore, the temperature where the physical network between the urea moieties is formed again upon cooling is shifted to lower temperatures. Additionally, the complex melt viscosity at 100 °C (η^*_{100}) for the polymers **1b**, **1c**, and **1d** ranges from 6390, 2030, and 610 Pa s whereas the melt viscosity of **1a** is above the limit of the available rheometer. Hence, it is obvious that η^* is proportional to the molecular weight and therefore the temperature range suitable for melt processing strongly depends on the molecular weight.

2.2. Melt Processing

2.2.1. Extrusion-Based Printing

EBP materials can be extruded by a filament, pneumatic, piston, or a screw driven system and enables the fabrication of continuous fibers from polymer melts for the creation

of 3D constructs. The diameter of the fibers depends on the nozzle size, the applied printing pressure, the melt viscosity of the polymer and the printing speed. Finding the right combination of these parameters enables the control of the fiber dimensions.

The synthesized $(AB)_n$ segmented copolymers were processed with EBP. As expected from rheology, **1a** and **1b** cannot be melt processed with the used 3D printer due to the high molecular weight and thus high melt viscosity. When **1c** was tested at 130 °C and 350 kPa (the limiting upper parameters of the 3D printer), a poor printing result with undefined fiber diameters was obtained. Only **1d** can be processed with EBP at the temperature of 120 °C. Isothermal viscosity measurement of **1d** at 100 and 120 °C revealed constant melt viscosities and no degradation (Figure 4B). Therefore, EBP was conducted with **1d** from this point. The layer-on-layer stacking of processed fibers was investigated by depositing ten straight layers onto each other. **Figure 5**A shows straight and well-positioned fibers, high stacking accuracy, and smooth surface and minimal defects. Additionally, square-patterned prints with varied number of layers were produced. A construct with two layers in *x*-direction and two in *y*-direction reveals excellent placing of fibers with an average diameter of 260 ± 10 µm (Figure 5B). Figure 5C shows a print with five layers in *x*-direction and five in *y*-direction resulting in a total of ten layers at the junction points. The average fiber diameter was determined to be 265 ± 6 µm demonstrating the high reproducibility of the print independent from the number of layers. Furthermore, the standard deviation is below 5% showing the well-placed fibers. This results in a constant pore size even at build height and allows the ideal assembly with bioinks by printing them into the pores. The physical interactions between the polymer chains result in the bonding at the junction points.

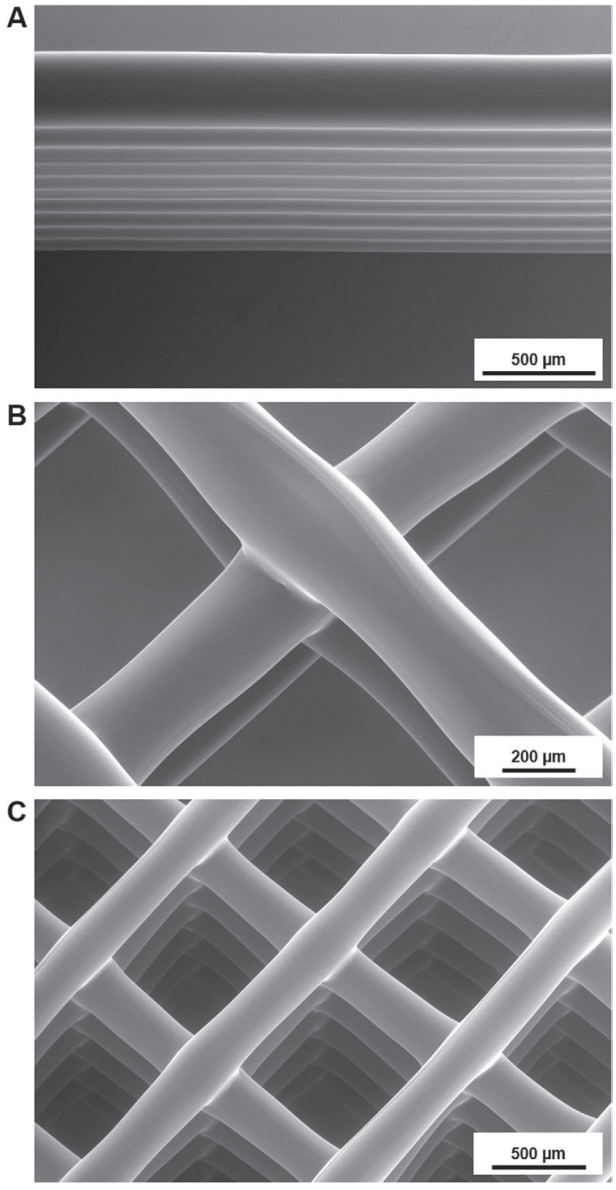

Figure 5. EBP of **1d** (printing parameters: temperature: 120 °C; pressure: 250 kPa; feed rate: 200 mm min^{-1}). A) Ten layers printed upon each other presenting the accurate stacking of polymer fibers. B/C) Prints with 2/5 layers in *x*-direction and 2/5 in *y*-direction, demonstrating the high printing accuracy, excellent stacking behavior, constant fiber diameter, smooth surface, and fiber bonding at the intersection points.

2.2.2. Melt Electrospinning

MES is a electrohydrodynamic fiber manufacturing technology for biomedical, filtration, and soft matter applications.[11] Resolution limits on the EBP due to die swell, as well as MEW can be overcome using MES technique that uses electrical instabilities to draw the jet to small dimensions. Fiber formation occurs from the cooling of polymer melts and allows manufacturing continuous ultrafine fibers that create a thin nonwoven constructs with a low micron architecture.[29] Upon the application of an electrical potential difference between a nozzle and collector, a polymer melt is ejected towards the collector as a small diameter jet. MES fabricates random oriented fibers similar to solution electrospinning using the mechanism of electrostatic repulsion and bending instabilities in fluid columns.[30] Numerous polymers can be used in MES including PLA, low-density polyethylene, poly(ethylene terephthalate), PCL, and PP. MES fiber diameters have been realized from submicron to many micrometers[31–33] depending on different parameters, such as pressure, molecular weight of polymer, temperature, applied voltage, and nozzle to collector distance.[34]

The influence of temperature (85, 95, 100 °C) and pressure (10, 20, 50 kPa) on the MES fiber diameter was investigated for **1d** (Figure S6, Supporting Information). Depending on the applied parameters, fiber diameters in a range of 0.8–15 µm were obtained. As shown in **Figure 6**, nonwoven constructs consisting of thin fibers were observed.

Due to the simplicity of forming ultrafine fibers using MES, there is a great interest in controlling electrospun fiber deposition to widen its potential application.

2.2.3. Melt Electrowriting

MEW can be considered as a hybrid fabrication technology of EBP and MES, although a distinct electrohydrodynamic

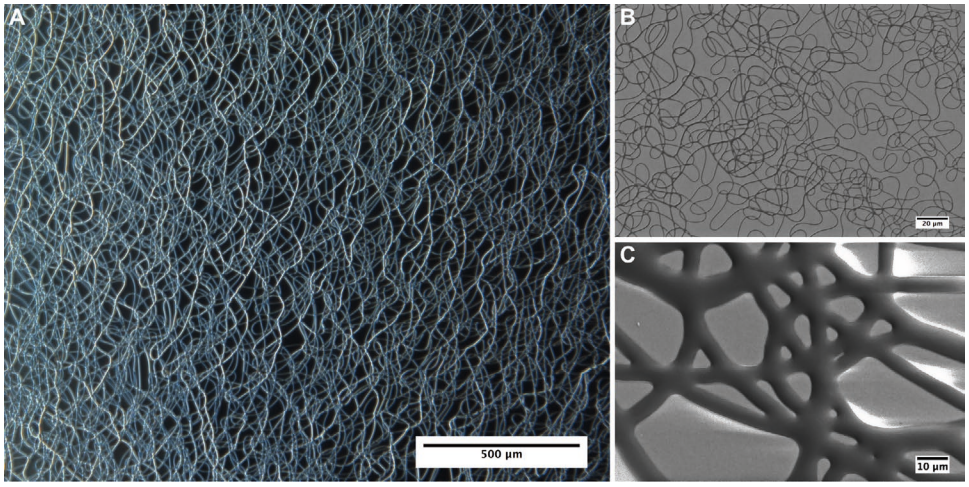

Figure 6. A) Representative of stereomicroscope image and B,C) Scanning electron microscope images of printed MES fibers on a glass collector using polymer **1d** (printing parameters of (A): temperature: 85 °C, pressure: 50 kPa, nozzle-collector distance: 21 mm, nozzle diameter: 0.3 mm, voltage: 16.5 kV. Printing parameters of (B): temperature: 85 °C, pressure: 10 kPa, nozzle-collector distance: 25 mm, nozzle diameter: 0.3 mm, voltage: 17.5 kV. Printing parameters of (C): temperature: 100 °C, pressure: 10 kPa, nozzle-collector distance: 25 mm, nozzle diameter: 0.3 mm, voltage: 18.5 kV).

phenomenon of jet stabilization enables the technique to work.[35] Since MEW can attain smaller printed diameters than EBP, it is an emerging technique for controlled deposition of highly resolved structures. Applying lower high voltages than MES results in a molten jet that remains stable and continuous. When direct-written over a collector, the molten jet rapidly cools.[36] The collector speed is the most important factor for the straightness of the fibers. The threshold speed where the direct written fiber converts from sinusoidal to linear is named critical translational speed (CTS).[16]

Polymer **1a** could not be melt-processed by MEW up to 210 °C. For **1b**, MEW was possible at 150 °C, though the obtained jet was inhomogeneous. Moderate processing temperatures of 95 and 85 °C were obtained for **1c** and **1d**, respectively. Therefore, MEW was conducted with these polymers. The influence of several instrumental parameters (printing temperature, voltage, feeding pressure, and collector speed) was investigated for single fibers for **1c** and **1d** from MEW. As shown in Figures S7 and S8, Supporting Information, the fiber diameter significantly decreases with increasing collector speed, decreasing temperature, and higher voltages. Similar tendencies were observed for previously MEW processed materials, such as PCL and $(AB)_n$ segmented copolymers based on poly(urea-siloxane).[14,16,28,37] Interestingly, the fiber diameter only increases with increasing feeding pressure below 50 kPa for **1c**. Approximately equal fiber diameters were obtained when printing with 50 and 100 kPa. It was also observed for **1d** at printing temperature of 85 °C. Depending on the applied parameters, fiber diameters in a range between 5 and 35 µm were obtained for both polymers.

Patterns of **1c** (Figure S9, Supporting Information) and **1d** (**Figure 7**) were printed via MEW. In Figure 7, uniform fibers with constant diameters and without any coiling, fiber pulsing or long-beading are shown for **1d**. The polymer **1d** was melt electrowritten as a tubular structure using cylindrical mandrel (Figure 7A,B). Fiber diameter was obtained 156 ± 3.8 µm from ten-layer structures with 45° winding angles. Tubular structures are promising for tracheal and cardiovascular tissue engineering applications. Interestingly, the square-shaped prints have a flat height revealing that the stacked fibers merged together (Figure 7C). This can be explained by the low distance between the hot nozzle and the polymer layers of only 2.2 mm leading to a slow solidification of the polymer. Additionally, the polymers have an inherent self-healing behavior. Consequently, larger fiber diameters of 66 ± 6 µm as compared to printed single fibers and small print heights were obtained.

AM is a versatile manufacturing approach, which allows the production of customized parts. With EBP, MES, and MEW, the polymer melts are processed and printed to form a final product. All four polymers were studied with EBP, MES, and MEW to determine the minimum temperatures T_{EBP}, T_{MES}, and T_{MEW} where a stable melt flow is possible. Polymer **1a** was not possible to print with EBP, MES, or MEW. **1b** could only be melt processed to some extent at 150 °C with MEW. Nevertheless, the obtained jet was inhomogeneous. Polymer **1c** could not be printed with the used printer for EBP, MES was not tested, and printing with MEW was possible at 95 °C (Figure S9, Supporting Information). The best printing results were achieved with **1d**. At 120 °C, accurate stacking of polymer fibers and prints with different layers demonstrating the high printing accuracy was shown with EBP (Figure 5). MES and MEW can be conducted at lower temperatures compared to EBP. Melt-processing of **1d** with MES and MEW was already possible at 85 °C. Processability was achieved within the temperature range from 85 to 100 °C (Figures 6 and 7). Polymer **1d** works well with all three used techniques. This demonstrates the influence of the molecular weight on the viscosity and the necessity to tailor the molecular weight for melt processing.

2.3. Swelling and Dissolution Behavior of the Bulk Material and Printed Constructs

$(AB)_n$ segmented copolymers with hydrophilic PEG-based segments are known for a high water uptake. They swell and form a

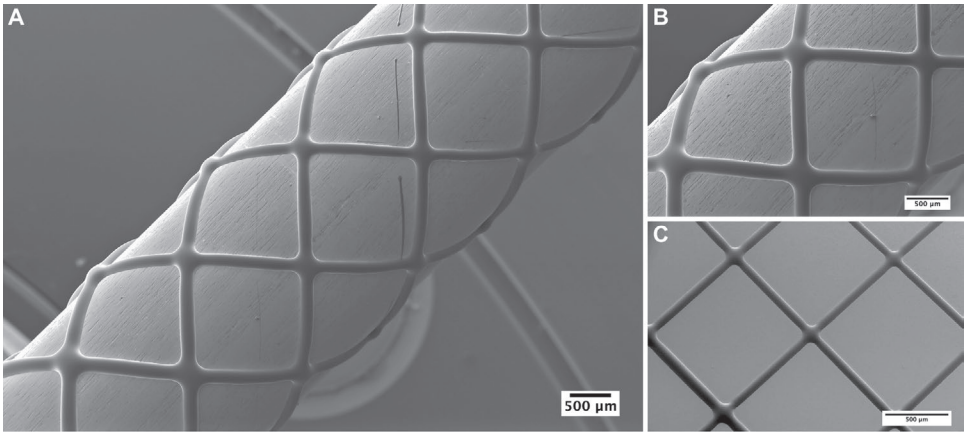

Figure 7. Scanning electron microscope images of MEW tubes on a A,B) cylindrical metal mandrel and C) glass using polymer **1d**. A,B) Ten-layer tubular print (printing parameters: temperature: 85 °C, nozzle-tubular collector distance: 2.55 mm, nozzle diameter: 0.41 mm, voltage: 3.3 kV, pressure: 120 kPa, efficient collector speed: 307.58 mm min^{-1}). The prints have uniform fibers with constant diameters that are flatten by self-healing property of this polymer class. C) Twenty layers (ten layers in *x*-direction and ten layers in *y*-direction) were printed on top of each other (printing parameters: temperature: 85 °C, nozzle-collector distance: 2.2 mm, nozzle diameter: 0.45 mm, voltage: 4.0 kV, pressure: 100 kPa, collector velocity: 1000 mm min^{-1}).

hydrogel for a certain period of time till they slowly disintegrate. In the following experiments, the water uptake and swelling behavior was observed and quantified. The time-dependent water uptake of the bulk material of **1d** was determined using a humidity balance. The water content reached an equilibrium of about 70 wt% after 24 h (**Figure 8**). The water content correlates well with different human soft tissues, such as skin, cartilage, and muscle, that all consist of around 70 wt% water.

Furthermore, the time-phased swelling behavior of the EBP processed ten-layer print from Figure 5C was studied by taking photographs of the full water-covered construct. Figure S10A, Supporting Information, reveals that the fibers of the printed polymer expand by taking up water, reducing the pore size. After 80 min, the pores are completely closed by the hydrogel while the geometry of the whole print remains stable.

Also, a structure with increasing distance between the strands was printed with EBP and **1d** as shown in **Figure 9**A. To determine the swelling behavior of the printed fibers in water, a time-lapse video was made and evaluated. The fibers swell by 525% within 180 min (Figure 9B; Figure S10B, Supporting Information).

2.4. Materials In View of Biofabrication

Biofabrication of tissue constructs offers to recapitulate the complexity of native tissues. It promises to create more practical in vitro model compared to traditional 2D systems or bulk scaffolds for different applications. To use $(AB)_n$ segmented copolymers in view of biofabrication, it is important to investigate the cytotoxicity of the polymers. Therefore, the viability of mouse fibroblasts cells in the presence of polymers **1c** and **1d** was studied by WST assay, CellTiter-Glo luminescent cell viability assay, and PicoGreen dsDNA assay. All cytotoxicity tests were conducted according to ISO-norm 10993-5. Polymer samples were prepared as smooth, thin films. More specifically, polymer films were melt pressed at 100 °C. Consequently, the material was already heated to a temperature range were AM can be conducted. The hydrogels were eluted in cell media with a concentration of 100 mg mL^{-1}. Additionally, diluted samples with 50% and 25% eluate were prepared. Materials are characterized as not cytotoxic if the viability of L929 CC1 mouse fibroblasts is above 80%. As shown in **Figure 10**, all three assays revealed high cell viability above 80% for both polymers and for all eluate concentrations including the lower end of the standard deviation. This result demonstrates that $(AB)_n$ segmented copolymers are not cytotoxic.

The used $(AB)_n$ copolymer class is promising for biofabrication that can be melt processed with three different methods. This approach allows creating different hierarchical structures for future studies. In addition, tunable mechanical properties of the $(AB)_n$ segmented copolymers make them a promising candidate for mimicking the mechanical and biological properties of different tissues.

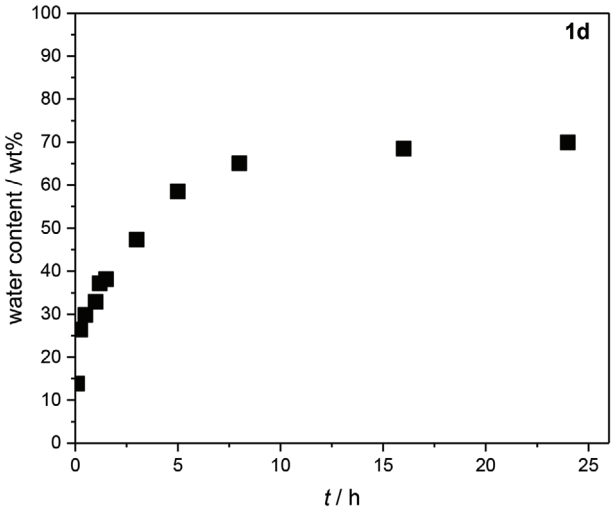

Figure 8. Time-dependent water uptake for 24 h at ambient temperature. The polymer absorbs around 70 wt% water.

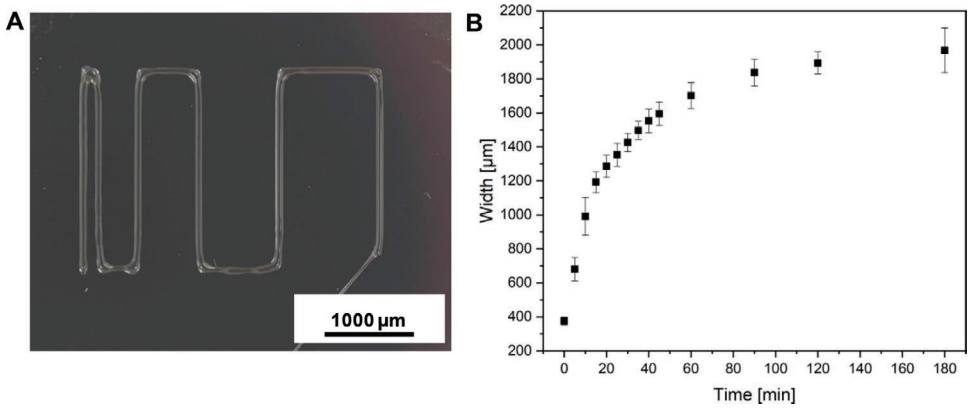

Figure 9. Swelling experiment of an extrusion-based printed structure with increasing distance between the strands A) printed with **1d**. B) Swelling of the fibers by 525% was reached after 180 min.

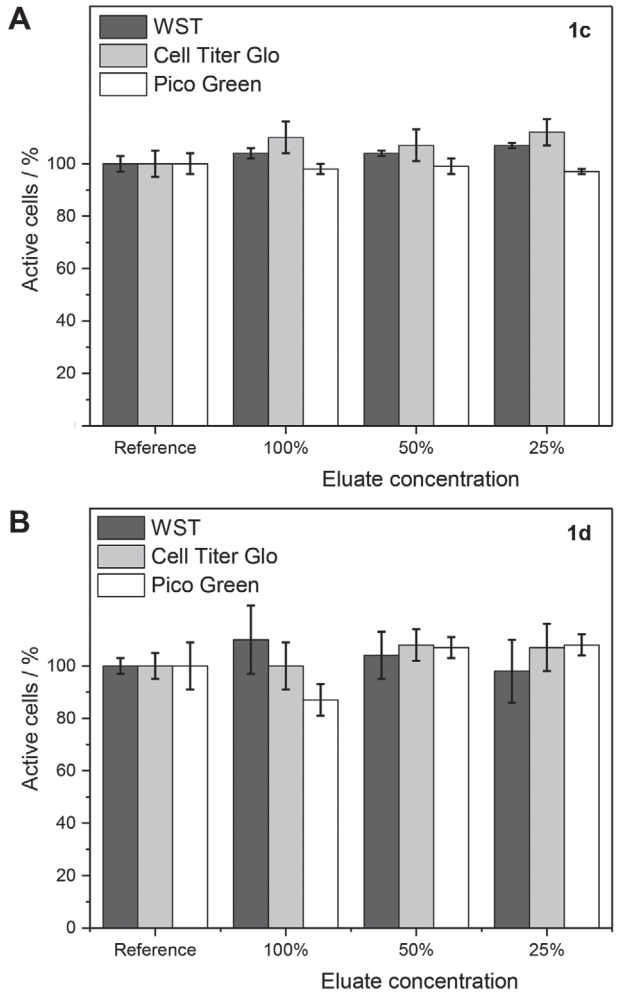

Figure 10. Viability of mouse fibroblast cells in the presence of A) **1c** and B) **1d** at three different eluate concentrations by performing WST, CellTiter-Glo, and PicoGreen assay. Hydrogel concentration in the eluate was 100 mg mL^{-1}. The viability is always above 80%, indicating that both polymers are not cytotoxic.

3. Conclusion

$(AB)_n$ segmented copolymers composed of hydrophilic PEG-based segments and hydrophobic bisurea segments can be tailored for processing from the melt with EBP, MES, and MEW. The formation of hydrogen bonds fosters interlayer bonding, allowing a wide range of patterns with different resolutions can be processed. This approach allows creating different hierarchical structures also in view of biofabrication with cytotoxicity tests that demonstrate the viability of cells and thus the biocompatibility of this class of physically crosslinked hydrogel.

4. Experimental Section

Film Preparation: Polymer films of 0.5–1 mm thickness were prepared by compression molding in a Carver 2512-2HC hot press. The films were heated to temperatures between 100 and 110 °C for 5 min and melt pressed between NOWOFLON PFA films by applying a pressure of 600 kPa. Then, the films were subsequently transferred into a Hi-Force cold press and pressed at 600 kPa upon cooling to room temperature. Required geometries were punched out of the polymer films and used for DMTA, rheology measurements, and water absorption experiments.

Differential Scanning Calorimetry: DSC measurements of dry polymers were performed on a Mettler Toledo DS2 device by using a sealed aluminum pan between –80 and 180 °C and under nitrogen atmosphere (50 mL min^{-1}). The first cooling and second heating cycle was measured with a rate of 10 K min^{-1}.

Dynamical Mechanical Thermal Analysis: Tension geometry DMTA measurements were performed on a Rheometric Scientific DMTA IV at a heating rate of 2 K min^{-1} and a frequency of 1 Hz. Samples with a thickness between 0.5 and 1 mm and a length of around 20 mm were used.

Melt Rheology: Oscillation and rotational rheology of the polymers was conducted using a Kinexus lab+ rheometer (Malvern Panalytical) at a heating and cooling rate of 2 K min^{-1} and a frequency of 1 Hz, rotational experiments at 0.08 rad. Samples with a thickness around 1 mm were investigated in a 25 mm plate–plate geometry. First cooling and second heating cycle were recorded.

Extrusion-Based Printing: A Cellink+ printer (AB Cellink) was used for the fabrication of 3D printed constructs. The device was controlled and programmed by HeartWare software (AB Cellink). The printer was equipped with an alumina cartridge and as a nozzle, a flat tipped cannula with a diameter of 0.40 mm was used. Only the cartridge was

heated. Hence, the cannula was shortened to avoid thermal loss and thus a clogging of the nozzle. The cartridge was filled with the $(AB)_n$ segmented copolymer **1d** and heated to 120 °C. The printing pressure was generated by an external compressor (Wiltec AF18 2). The pressure was adjusted to 250 kPa. The vertical position (*z*-axis) was calibrated to the height of a silicon wafer slice. The constructs were printed on the surface of the silicon wafer with a feed rate of 200 mm min^{-1}.

Melt Electrospinning and Melt Electrowriting: A custom-built MEW device was used as previously described.[28] MES and MEW were performed at 20 ± 2 °C and a relative humidity of 30% ± 5%. The polymer was heated at least for 15 min before experiment. The effect of different pressures and temperatures on single fiber diameters was systematically investigated for MES and MEW. The temperature and pressure were varied from 85 to 105 °C and 10 and 100 kPa, respectively. A flat tipped printing nozzle was positioned above either a glass microscope slide, a silicon wafer slice, or a cylindrical metal mandrel. The surface was moved under the charged nozzle using two computer-controlled linear axes (*x* and *y*). The circle pattern was used for MES. Squared-patterned prints were melt electrowritten by altering layer deposition in horizontal (*x*) and vertical (*y*) directions with turning loops. Tubular prints were melt electrowritten on cylindrical metal mandrels using 45° winding angle.

Swelling Tests: For the determination of the percentage of water in the hydrogel, the dry polymer was partitioned into several pieces of comparable size. The pieces were swollen in the equal amount of water for various durations ranging from 6 min to 24 h. After transferring the sample into a humidity balance (MA145 Sartorius), the hydrogel was dried at 120 °C until constant weight was reached. The water content of the swollen hydrogel w was then calculated from the mass of the swollen polymer m_s and the dried polymer m_d by using the following equation

$$w = \frac{m_s - m_d}{m_d} \times 100 \quad (1)$$

For the swelling experiment, a one-layered structure with increasing spacing between the printed strands was fabricated with a Cellink+ bioprinter (AB Systems). The structure was exposed to water at ambient conditions and the swelling was monitored and recorded by a Z-Cam E2 equipped with a 42 mm macro lens. A time-lapse video with an interval of 5000 ms and a frame rate of 25 fps was prepared and processed using Adobe Premiere Pro. The line widths after a certain period of time were determined by using ImageJ.

Biocompatibility/Cytotoxicity Tests: Cytotoxicity tests were conducted according to ISO 10993-5 applying L929 CC1 (ATCC, Rockville, USA) mouse fibroblasts cells. Polymer films were swollen in cell culture media consisting of Dulbecco's modified Eagle's medium GlutaMax, 1% 1 M HEPES, 1% penicillin–streptomycin, and 10% FCS. Hydrogel concentration was 100 mg mL^{-1}. PVC platelets were used for positive control. Pure elution medium served as negative control. Eluates were incubated for 48 h at 37 °C. Then, suspended sediments were centrifuged, and 100% eluate was prepared using the supernatant. 50% and 25% eluates were prepared by dilution with cell culture media. WST, PicoGreen, and CellTiter-Glo Luminescent Cell Viability assays were performed to determine the number of active cells. All samples were tested as triplicate.

Optical Microscopy: The average fiber diameter and deviation were measured by using the optical microscope (Standard Microscope Olympus BX60) or the stereomicroscope (Discovery V20, Carl Zeiss Microscopy GmbH), in the reflected light modus and calculated by using the software ImageJ for MEW samples.

Scanning Electron Microscopy: A Crossbeam 340 scanning electron microscope equipped with GEMINI e-Beam column (Carl Zeiss Microscopy) and the scanning electron microscope FEI Quanta FEG 250 (Thermo Fisher Scientific) were used for measurement of fiber diameter of MES samples and imaging of printed constructs. Non-coated samples were imaged with the Crossbeam 340 scanning electron microscope using secondary electrons (SE) at 2 kV. The untreated fabricated materials were placed in the sample chamber of the FEI Quanta FEG 250 and the measurements of the prints were conducted in the low vacuum mode by applying a chamber pressure of 40 Pa.

Supporting Information

Supporting Information is available from the Wiley Online Library or from the author.

Acknowledgements

Funding was provided by the German Research Foundation (DFG)—project number 326998133—SFB TRR225 (subproject A04). The Elite Study Program Macromolecular Science within the Elite Network of Bavaria (ENB) and the Keylab Small Scale Polymer Processing of the Bavarian Polymer Institute at the University Bayreuth are gratefully acknowledged for their support. The authors thank Michael Bartolf-Kopp for technical assistance. In the original publication of this article, the abstract ended with the word "demonstrated" after the word "copolymers". This was a mistake, and was removed on January 7, 2021, after initial online publication of this article.

Open access funding enabled and organized by Projekt DEAL.

Conflict of Interest

The authors declare no conflict of interest.

Keywords

3D printing, $(AB)_n$ segmented copolymers, biocompatibility, melt electrowriting

Received: August 12, 2020
Revised: September 28, 2020
Published online: November 23, 2020

[1] B. Brenken, E. Barocio, A. Favaloro, V. Kunc, R. B. Pipes, *Addit. Manuf.* **2018**, *21*, 1.
[2] S. Negi, A. A. Nambolan, S. Kapil, P. S. Joshi, R. Manivannan, K. P. Karunakaran, P. Bhargava, *Rapid Prototyping J.* **2019**, *26*, 485.
[3] W. Ameen, A. M. Ghaleb, M. Alatefi, H. Alkhalefah, A. Alahmari, *Virtual Phys. Prototyping* **2018**, *13*, 282.
[4] A. Youssef, S. J. Hollister, P. D. Dalton, *Biofabrication* **2017**, *9*, 012002.
[5] J. T. Cantrell, S. Rohde, D. Damiani, R. Gurnani, L. DiSandro, J. Anton, A. Young, A. Jerez, D. Steinbach, C. Kroese, P. G. Ifju, *Rapid Prototyping J.* **2017**, *23*, 811.
[6] E. G. Gordeev, A. S. Galushko, V. P. Ananikov, *PLoS One* **2018**, *13*, e0198370.
[7] M. Jin, C. Neuber, H.-W. Schmidt, *Addit. Manuf.* **2020**, *33*, 101101.
[8] I. Zein, D. W. Hutmacher, K. C. Tan, S. H. Teoh, *Biomaterials* **2002**, *23*, 1169.
[9] M. Vaezi, S. Yang, *Virtual Phys. Prototyping* **2015**, *10*, 123.
[10] N. Kishi, H. Iizuka, *Polym. Lett.* **1964**, *2*, 399.
[11] T. M. Robinson, D. W. Hutmacher, P. D. Dalton, *Adv. Funct. Mater.* **2019**, *29*, 1904664.
[12] R. Nayak, R. Padhye, I. L. Kyratzis, Y. B. Truong, L. Arnold, *Text. Res. J.* **2013**, *83*, 606.
[13] G. Hochleitner, T. Jüngst, T. D. Brown, K. Hahn, C. Moseke, F. Jakob, P. D. Dalton, J. Groll, *Biofabrication* **2015**, *7*, 035002.

[14] T. D. Brown, P. D. Dalton, D. W. Hutmacher, *Adv. Mater.* **2011**, *23*, 5651.
[15] F. M. Wunner, M.-L. Wille, T. G. Noonan, O. Bas, P. D. Dalton, E. M. De-Juan-Pardo, D. W. Hutmacher, *Adv. Mater.* **2018**, *30*, 1706570.
[16] G. Hochleitner, A. Youssef, A. Hrynevich, J. N. Haigh, T. Jungst, J. Groll, P. D. Dalton, *BioNanomaterials* **2016**, *17*, 2387.
[17] J. Malda, J. Visser, F. P. Melchels, T. Jüngst, W. E. Hennink, W. J. A. Dhert, J. Groll, D. W. Hutmacher, *Adv. Mater.* **2013**, *25*, 5011.
[18] F. P. W. Melchels, M. A. N. Domingos, T. J. Klein, J. Malda, P. J. Bartolo, D. W. Hutmacher, *Prog. Polym. Sci.* **2012**, *37*, 1079.
[19] J. S. Miller, K. R. Stevens, M. T. Yang, B. M. Baker, D.-H. T. Nguyen, D. M. Cohen, E. Toro, A. A. Chen, P. A. Galie, X. Yu, R. Chaturvedi, S. N. Bhatia, C. S. Chen, *Nat. Mater.* **2012**, *11*, 768.
[20] A. Nadernezhad, N. Khani, G. A. Skvortsov, B. Toprakhisar, E. Bakirci, Y. Menceloglu, S. Unal, B. Koc, *Sci. Rep.* **2016**, *6*, 33178.
[21] J. Groll, T. Boland, T. Blunk, J. A. Burdick, D.-W. Cho, P. D. Dalton, B. Derby, G. Forgacs, Q. Li, V. A. Mironov, L. Moroni, M. Nakamura, W. Shu, S. Takeuchi, G. Vozzi, T. B. F. Woodfield, T. Xu, J. J. Yoo, J. Malda, *Biofabrication* **2016**, *8*, 013001.
[22] P. Y. W. Dankers, M. J. A. van Luyn, A. Huizinga-van der Vlag, G. M. L. van Gemert, A. H. Petersen, E. W. Meijer, H. M. Janssen, A. W. Bosman, E. R. Popa, *Biomaterials* **2012**, *33*, 5144.
[23] M. Guo, L. M. Pitet, H. M. Wyss, M. Vos, P. Y. W. Dankers, E. W. Meijer, *J. Am. Chem. Soc.* **2014**, *136*, 6969.
[24] G. M. Pawar, M. Koenigs, Z. Fahimi, M. Cox, I. K. Voets, H. M. Wyss, R. P. Sijbesma, *Biomacromolecules* **2012**, *13*, 3966.
[25] Y. Cui, M. Tan, A. Zhu, M. Guo, *J. Mater. Chem. B* **2014**, *2*, 2978.
[26] T. D. Brown, P. D. Dalton, D. W. Hutmacher, *Prog. Polym. Sci.* **2016**, *56*, 116.
[27] C. L. Rohn, *Analytical Polymer Rheology: Structure, Processing, Property Relationships*, Hanser, Munich **1995**.
[28] G. Hochleitner, E. Fürsattel, R. Giesa, J. Groll, H.-W. Schmidt, P. D. Dalton, *Macromol. Rapid Commun.* **2018**, *39*, 1800055.
[29] M. L. Muerza-Cascante, D. Haylock, D. W. Hutmacher, P. D. Dalton, *Tissue Eng., Part B* **2015**, *21*, 187.
[30] C. J. Luo, S. D. Stoyanov, E. Stride, E. Pelan, M. Edirisinghe, *Chem. Soc. Rev.* **2012**, *41*, 4708.
[31] E. Zhmayev, D. Cho, Y. L. Joo, *Polymer* **2010**, *51*, 4140.
[32] N. Ogata, N. Shimada, S. Yamaguchi, K. Nakane, T. Ogihara, *J. Appl. Polym. Sci.* **2007**, *105*, 1127.
[33] L.-H. Zhang, X.-P. Duan, X. Yan, M. Yu, X. Ning, Y. Zhao, Y.-Z. Long, *RSC Adv.* **2016**, *6*, 53400.
[34] J. Lyons, C. Li, F. Ko, *Polymer* **2004**, *45*, 7597.
[35] P. D. Dalton, *Curr. Opin. Biomed. Eng.* **2017**, *2*, 49.
[36] T. D. Brown, F. Edin, N. Detta, A. D. Skelton, D. W. Hutmacher, P. D. Dalton, *Mater. Sci. Eng., C* **2014**, *45*, 698.
[37] A. Hrynevich, B. Ş. Elçi, J. N. Haigh, R. McMaster, A. Youssef, C. Blum, T. Blunk, G. Hochleitner, J. Groll, P. D. Dalton, *Small* **2018**, *14*, 1800232.